ChemCatChem

The European Society Journal for Catalysis

Chemistry Europe

European Chemical Societies Publishing

Supported by GECATS GERMAN CATALYSIS SOCIETY

Accepted Article

Title: Direct Z-scheme among Niobium Pentoxide and Poly(heptazine imide) for NH3 Photoelectrosynthesis under Ambient Conditions

Authors: Sirlon F. Blaskievicz, Ivo Freitas Teixeira, Lucia Helena Mascaro, and Juliana Ferreira de Brito

To be cited as: *ChemCatChem* **2023**, e202201610

Link to VoR: https://doi.org/10.1002/cctc.202201610

WILEY-VCH

WILEY-VCH

RESEARCH ARTICLE

Direct Z-scheme among Niobium Pentoxide and Poly(heptazine imide) for NH_3 Photoelectrosynthesis under Ambient Conditions

Dr. Sirlon F. Blaskievicz[a], Prof. Ivo Freitas Teixeira[a], Prof. Lucia Helena Mascaro*[a] and Prof. Juliana Ferreira de Brito*[b]

[a] Dr. Sirlon F. Blaskievicz, Prof. Ivo Freitas Teixeira, Prof. Lucia Helena Mascaro
Department of Chemistry
Federal University of São Carlos - UFSCar– twitter: @ufscaroficial
Rod. Washington Luiz, Km 235
13565-905, São Carlos (Brazil)
E-mail: lmascaro@ufscar.br; https://www.dq.ufscar.br/docentes/lucia-helena-mascaro-sales

[b] Prof. Juliana Ferreira de Brito
Alternative Technologies of Detection, Toxicological Evaluation and Removal of Micropollutants and Radioactives (INCT-DATREM), Institute of Chemistry
Universidade Estadual Paulista (UNESP) – twitter: @IqUnesp
14800-900, Araraquara (Brazil)
E-mail: juliana.f.brito@unesp.br; https://unesp.br/portaldocentes/docentes/270748

Supporting information for this article is given via a link at the end of the document.

Abstract: There is a crescent need to improve well-known processes to environmentally friendly options, and NH_3 production is not an exception. Herein, we describe the photoelectrochemical nitrogen reduction reaction under a carbon nitride, the poly(heptazine imide) (PHI) using mild conditions for NH_3 synthesis. For this purpose, PHI was combined with Nb_2O_5 nanotubes, leading to a new photocathode with a charge transfer process in a Z-scheme structure. The photoelectrocatalytic N_2 reduction was carried out in Nb_2O_5Nt/PHI using solar-simulated radiation and with an applied bias of −0.3 $V_{Ag/AgCl}$. The PHI presence in the photocathode showed not only superior stability compared to bare Nb_2O_5, but also an ammonia generation rate of 0.156 mmol L^{-1} h^{-1} cm^{-2}, which is about 10-fold higher than the amount obtained with niobium oxide alone. The mild and green conditions employed for ammonia generation place the obtained photocathode as a promising option for the currently used Haber-Bosch process.

Introduction

Once ammonia is a low-carbon fuel, an energy carrier, and a commodity in the global industry of fertilizer, the motivation to search for greener methods able to substitute the Haber Bosh process in the NH_3 synthesis has been driving many studies.[1,2] The required nitrogen repositions, associated with the degradation of agriculturally usable soil for high-yield nutritious crop obtention, are strictly dependent on the addition of fertilizers[3,4]. In this sense, the need for NH_3 production increases in the same order as the growing global population. Then, abundant and low-cost NH_3 production plays a central role to provide an affordable and stable food supply for the global population. The main motivation to replace the current Haber Bosh process is that this method releases 2.6 tons of greenhouse gas per 1 ton of generated NH_3.[5] Thus, techniques such as photocatalysis,[6,7] electrocatalysis,[8,9] and photoelectrocatalysis[10,11] to convert N_2 to NH_3 using mild conditions had stood out in the literature. In this way, it is possible to assure an energy-saving and low-pollution method for the synthetic ammonium industry, benefiting the fertilizer and textile industries.[2] The main target of those research is to obtain an efficient, robust, and stable catalyst. Many options and combinations of materials have been investigated in this sense.

Taking the photoelectrocatalysis technique into consideration, some of the most favorable materials reported in the literature are based on heterojunctions. In this sense, the nanostructures seem to be the most promisor choice. Ye and coworkers[11] have been investigating the nanojunction structure of MoS_2 nanosheet-assembled TiO_2 nanoparticles to be used as a photocathode in the photoelectroshyntesis of ammonia. The N_2 conversion to NH_3 using photoelectrocatalysis was also reported using hierarchical flower-like $MoSe_2$@g-C_3N_4 micro/nanostructures[12]. Additionally, the combination of materials has been investigated, such as Sb_2Se_3 modified with Pt nanoparticles,[10] and a boron-doped g-C_6N_6 layer.[13]

Among the nanostructure possibilities for photoelectrodes, the nanotubular is a prosperous option for photocatalytic reactions.[14] Metal oxide nanotubular arrays are known for their many valuable properties, such as high surface area, an elevated number of active sites, high and fast charge separation and transfer, photocorrosion resistance, chemical stability, and so on.[15–17] Concerning photocatalytic application, the density of bulk states is usually much higher for nanotubular morphology than for conventional nanoparticles.[18] The most stable phase among niobium oxides, the niobium pentoxide (Nb_2O_5), presents those characteristics under a nanotubular array.[19] It is an n-type semiconductor with energy absorption in the UV region (band gap around 3.4 eV).[20] Those characteristics make the niobium pentoxide nanotubes (Nb_2O_5Nt) suitable to be used as a platform for the deposition of other semiconductors, generating homo or heterojunctions that can be effective for redox reactions.

Another promising class of material is nitrogen-rich compounds, such as nitrogen-dopped carbon and polymeric carbon nitrides (PCN). Due to its highly polarizable structure, nitrogen-rich compounds improve the N_2 adsorption, and subsequently, the dissociation for ammonia formation.[21] The electron-rich nitrogen and/or carbon atoms can also act as Lewis basic sites, which leads to a frustrated Lewis pair (FLP), further leading to strong

activation of N_2 molecules by electronic polarization.[22] Oschatz *et al.* employed N-doped porous carbon support for electrochemical nitrogen reduction reaction (N2RR) over gold single sites, where a cooperative effect between the metal and the support was observed, with the gold sites modulating the electronic properties of the support, leading to an enhanced N2RR. Despite the good conductive structure proper for electrocatalysis, PCN also shows a band gap of around 2.7 eV, which is suitable for solar energy harvesting.[23] Combining the PCN photoactivity with the above-cited properties of nitrogen-rich compounds, PCN structures were investigated for photocatalytic reactions,[24] with a potential for photoelectrocatalytic ammonia generation.

Herein we report the synthesis and application of a poly(Heptazine Imide) (PHI) in combination with Nb_2O_5 nanotubes (Nb_2O_5Nt/PHI) for the N2RR by photoelectrosynthesis, with the production of ammonium, using a solar light simulator under mild conditions. The mechanism for the activation of the photocatalyst, charge transfer process, and NH_3 production was also proposed.

Results and Discussion

Characterization

The morphological structure of the Nb_2O_5 nanotubes with and without PHI modification is presented in Figure 1. The top-view SEM image in Figure 1A shows a surface with well-distributed and self-organized nanotubes. The average length of the nanotubes is 2.4 μm, while the average internal diameter is 45 nm, and the average wall thickness is 11.5 nm, as can be observed in companion work.[14] The inset of Figure 1a shows a cross-section image with the nanotube length confirming that the nanotubular structure was formed and not only a multivacancy structure. The mapping of chemical elemental distribution of this sample (Figure 2A) shows the presence of just Nb and O, proving that the nanotubes are composed by niobium oxides (Nb_2O_5), as expected. After the deposition of PHI in the Nb_2O_5 nanotubes, the surface turned to be covered by a thin film with a few agglomerated regions (Figure 1B). Chen *et al*[25] have demonstrated that the PHI is organized in nanocrystalline units forming a mesocrystal arrangement with sheet-like morphology. The mapping of chemical elemental distribution for this case (Figure 2B) indicates a uniform distribution of Nb, O, Na, and N atoms throughout the entire surface of the photocatalyst. The Na presence is expected once the synthesis employed results in negative-charged nitrogen in the PHI structure, stabilized by sodium ions.[25] The small amount of Na and N compared with Nb and O also indicates the formation of the Nb_2O_5Nt/PHI catalyst heterojunction.

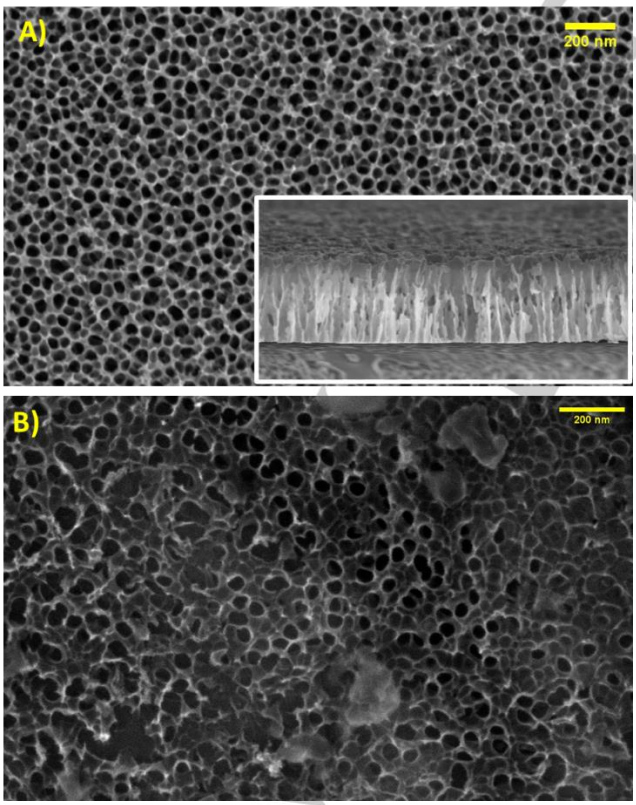

Figure 1. SEM images for the A) top view of Nb_2O_5Nt with an inset of the cross-section and B) top view of Nb_2O_5Nt/PHI.

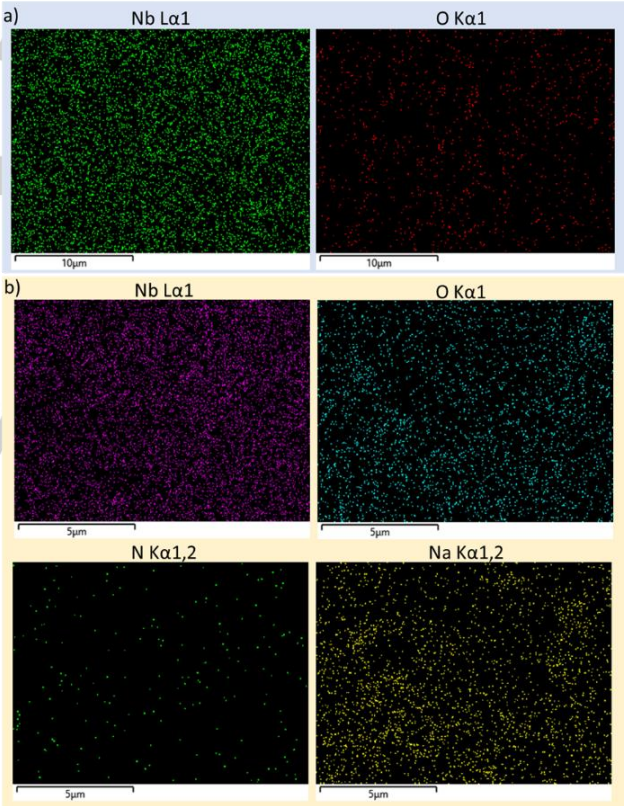

Figure 2. Elemental mapping analysis of each element present in the a) Nb_2O_5Nt and b) Nb_2O_5Nt/PHI photocatalysts.

Figure 3 exhibits XRD and Raman characterizations for the photoelectrodes Nb_2O_5Nt and Nb_2O_5Nt/PHI. The XRD data presented in Figure 3a allows for attaining structural information about the samples. The fact that just a thin film of PHI is deposited on the Nb_2O_5Nt surface, as can be confirmed by the mapping of chemical elemental distribution (Figure 2B), and that the main peaks of PHI have a near position concerning the main peak of the Nb_2O_5Nt, drove to an identification of just the peak at 2θ =

25.6 related to the presence of the polymer. The other well-defined peaks are related to the high crystalline phases of the typical orthorhombic structure of Nb_2O_5Nt indexed using JCPDS card no. 30–0873.[19] The XRD for just PHI deposited using the same methodology but on FTO with a higher number of layers can be observed in Figure S1. The main feature of PHI is a broad peak between 25 and 28° corresponding to the (002) plane of the stacked graphitic layered PHI (Figure S1),[27] which is observed in Figure 3A (peak at 25° indicated by an asterisk). The peak at 8.28° is related to the (100) plane, from the hexagonal arrangement of the heptazine units,[25] and the polymerized structures within the layers (plane (110)) are observed in the peak at 14.3° (Figure S1).[25,26] Finally, there are no diffraction peaks related to any impurities of the material.

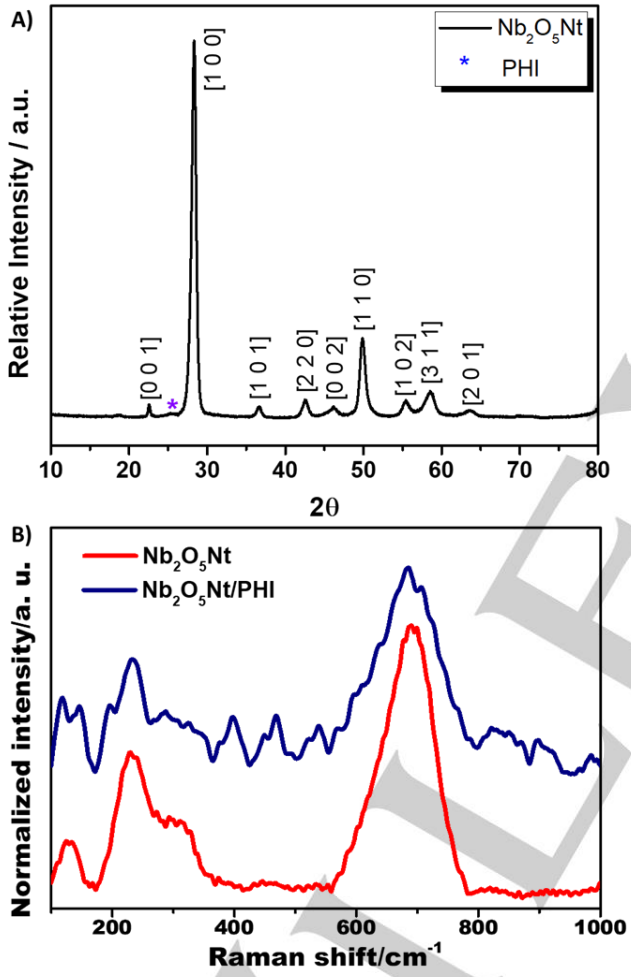

Figure 3. A) XRD diffractogram of Nb_2O_5Nt/PHI and B) Raman spectra of Nb_2O_5Nt (red line) and Nb_2O_5Nt modified with PHI (blue line).

The microstructure was investigated through Raman spectroscopy shown in Figure 3B. As observed in the XRD, the crystallinity of the sample is evidenced by the clear and well-defined bands of Nb_2O_5Nt (red line). In both bare and coated samples, the broadband at ca. 690 cm^{-1} is related to the low distorted octahedral NbO_6 coordination.[28,29] The bands observed in about 220 and 310 cm^{-1} respectively corresponded to the bending vibration of Nb-O-Nb, and it is a fingerprint of the Nb_2O_5 orthorhombic structure.[30] The weak band at 850 cm^{-1} in turn, can be attributed to the Nb=O stretching mode. When coated with PHI, features related to carbon nitride were observed, such as C-N vibrational modes in the range of ~380 – 580 cm^{-1},[31] as well the in-plane bending vibrations of the heptazine linkages above 900 cm^{-1} and the ring breathing mode, observed in ~980 cm^{-1}.[32] Those results (Figures 1 to 3) corroborate the confirmation of the Nb_2O_5Nt/PHI photocatalyst formation.

To evaluate how the PHI deposition interferes with the charge transfer resistance (R_{ct}), electrochemical impedance spectroscopy (EIS) measurements under dark and assisted by light incidence were carried out for Nb_2O_5Nt and Nb_2O_5Nt/PHI (Figure 4). The results were adjusted using a Randles equivalent circuit. As expected, both semiconductors presented a high resistive behavior (in the order of kΩ) under dark conditions. The R_{ct} values obtained for both photocatalysts under the dark (inset Figures 4A and 4B) were close to each other (89.37 and 86.94 kΩ cm^{-2} for Nb_2O_5Nt and Nb_2O_5Nt/PHI respectively). On the other hand, under light radiation, the resistance decreased drastically for both materials, with the formation of two semicircles, one in the high-frequency range with small intensity and the other at lower frequency values with large intensity (Figure 4). Is possible to observe the limitation of a diffusional process for both samples during illumination, but less significatively for Nb_2O_5Nt/PHI as seen by the small slope in lower frequencies (Figure 4b). The

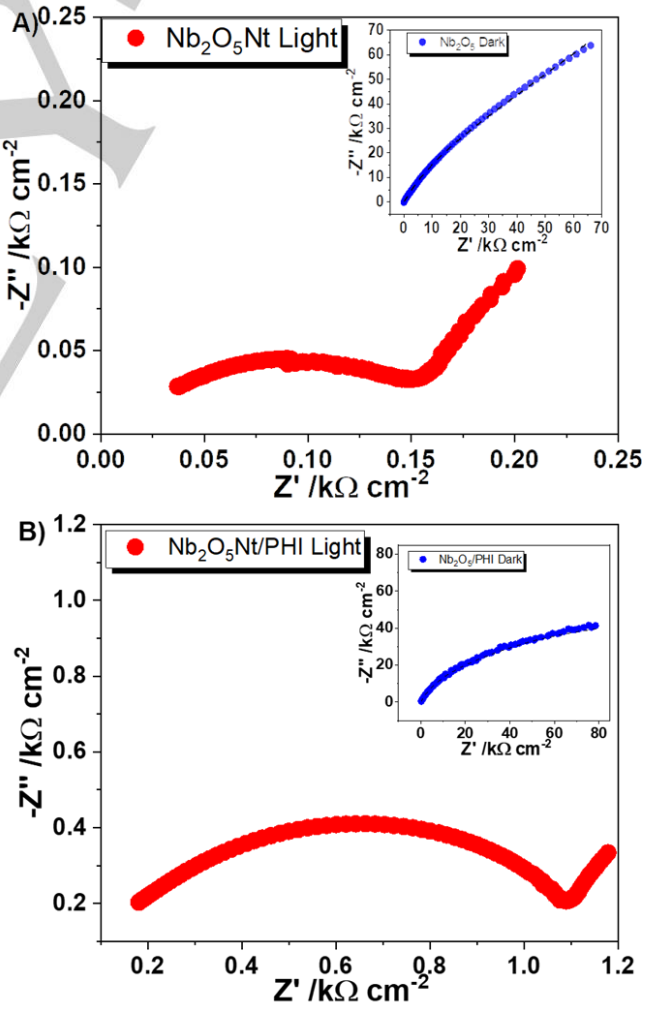

Figure 4. EIS spectra under dark (blue dots) and 1 sun (red dots) conditions for **A)** Nb_2O_5Nt and **B)** Nb_2O_5Nt/PHI, the dashed lines correspond to the equivalent circuit fit, in PBS buffer.

small semicircle refers to the resistance and pseudo-capacitance of the charge transfer process.[33,34] A larger radius indicates higher R_{ct} values, and, in the sample with and without PHI, it was found to be 248.66 and 159.86 Ω cm^{-2}, respectively. Unlikely other polymeric semiconductors, PHI did not present good electrical conductivity even under light, which justifies the increase in R_{ct}, in addition to a possible surface area reduction, as the PHI deposition covers the surface of the nanotubes. This hypothesis is reinforced due to the flattened arc observed in the Nb_2O_5Nt samples, characteristic of the rough character of the electrode interface. Anyhow, the N_2 reduction process is dependent on many factors than the resistance, and, as will be seen further, this increase in R_{ct} did not significantly influence the reaction.

The flat band potential (E_{FB}) for both materials, Nb_2O_5Nt and Nb_2O_5Nt-PHI was calculated by Mott-Schottky measurements, from the extrapolation of the tangent line of the plot to the x-axis (Figure 5a). Following the literature, the Nb_2O_5Nt present characteristics of an n-type semiconductor,[35] with a positive slope of the plot, which is maintained after the modification with PHI. For n-type materials, the E_{FB} is near the conduction band (CB) position, due to the Helmholtz capacitance in dielectric semiconductors.[36] The E_{FB} value for the pristine Nb_2O_5 was -0.42 V vs Ag/AgCl (black line), which showed a small shift (-0.47 V vs Ag/AgCl) after being combined with PHI (red line). A band bending resulting from the CB of PHI being more negative.[27] Based on that, and in the band gap values, Figure 4B presents the position of both VB and CB for the Nb_2O_5Nt and the Nb_2O_5Nt/PHI heterojunction. Considering the position of the bands presented in the diagram, and the reduction potential of N_2 to NH_3 (0.092 V vs RHE), the photocatalyst is suitable to perform the N2RR, and it is proposed that the heterostructure is acting as a Z-Scheme charge transfer[37] providing the electrons to the N_2 reduction in the PHI surface, as will be discussed further ahead.

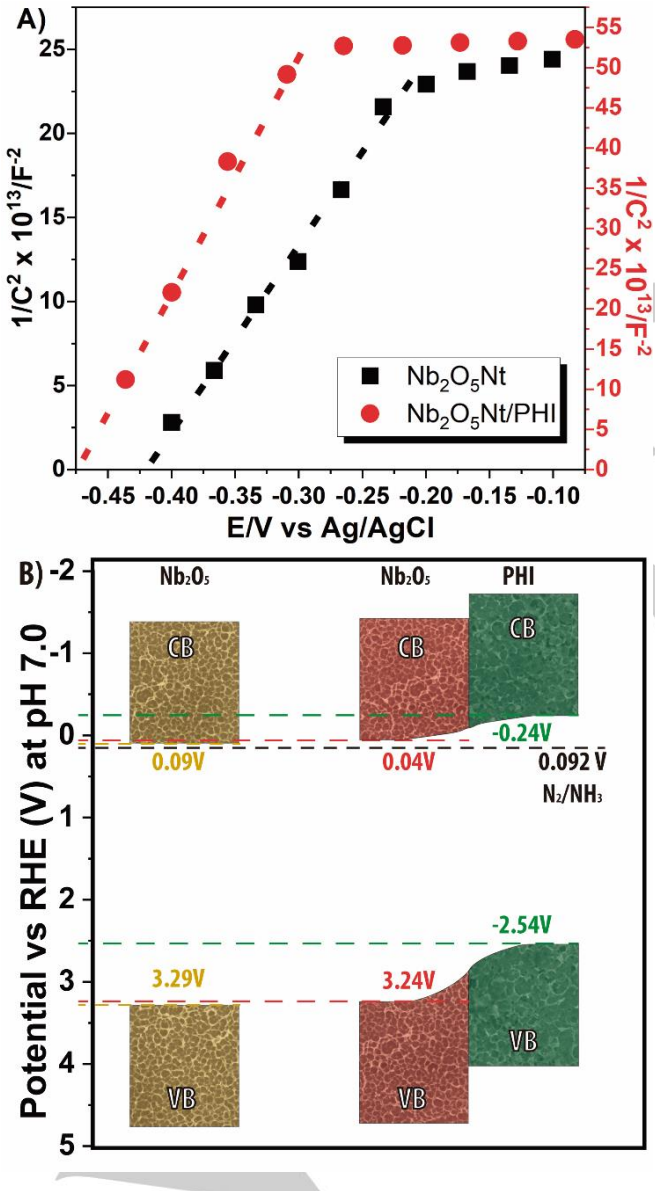

Figure 5. A) Mott-Schottky analysis of pure Nb_2O_5Nt (black) and Nb_2O_5Nt/PHI (red); **B)** Band position for the semiconductor alone and the heterojunction.

N_2 reduction

The behavior of the Nb_2O_5Nt with and without modification under light incidence during linear sweep voltammetry is presented in Figure 6. Once Nb_2O_5Nt is an n-type semiconductor, it is expected that the photocatalyst just presents anodic photocurrent,[14,38] as observed in Figure 6a. The irradiation of light in the Nb_2O_5Nt electrode under negative bias potentials can induce a shift in the current density only after the modification of the surface with PHI (Figure 6b). The Nb_2O_5Nt/PHI semiconductor presented similar behavior in the current density under dark and light incidence using PBS buffer saturated with N_2. However, after the incidence of light on the semiconductor surface, instead of a more negative photocurrent density, it is observed a shift of the photocurrent to fewer negative values. This behavior indicates the adsorption of N_2 on the PHI surface, favored by the electron/hole pairs generated from the activation of the semiconductor by photons with energy equal to or greater than the catalyst band gap, culminating in a decrease of available sites and, consequently, a decrease in the current when compared to the catalyst under dark.[10,39]

The cathodic photocurrent density for the photoelectrode Nb_2O_5Nt without modification starts after -0.2 $V_{(Ag/AgCl,3M)}$, without any appreciable difference from the dark and light data. This value changes for -0.1 $V_{(Ag/AgCl,3M)}$ under light incidence after the coating with PHI, while the OCP potential value for the catalysts changes from -0.28 to -0.18 $V_{(Ag/AgCl,3M)}$ with the deposition of PHI. Additionally, there is a discreet peak in the current registered for Nb_2O_5/PHI photocatalyst (Figure 6b) that changes to less negative potential when the semiconductor is activated by the incidence of light. Under dark, the peak is located at −0.31 $V_{(Ag/AgCl,3M)}$ while after light irradiation the peak is dislocated to −0.27 $V_{(Ag/AgCl,3M)}$. The absence of this peak when the photocatalyst is submitted to the LSV under supporting electrolyte saturated with Ar gas (inset Figure 6b) leads to conclude that there is an adsorption of N_2 in the photocatalyst surface, after the modification with PHI, which happens in potential around -0.3 $V_{(Ag/AgCl,3M)}$. This shift of the photocurrent to less negative potentials compared to the dark current is a common behavior of p-type or p-n junction semiconductors.[40–42] Those behaviors are in agreement with the modification promoted in the Nb_2O_5Nt, turning it suitable for application in the N_2RR.

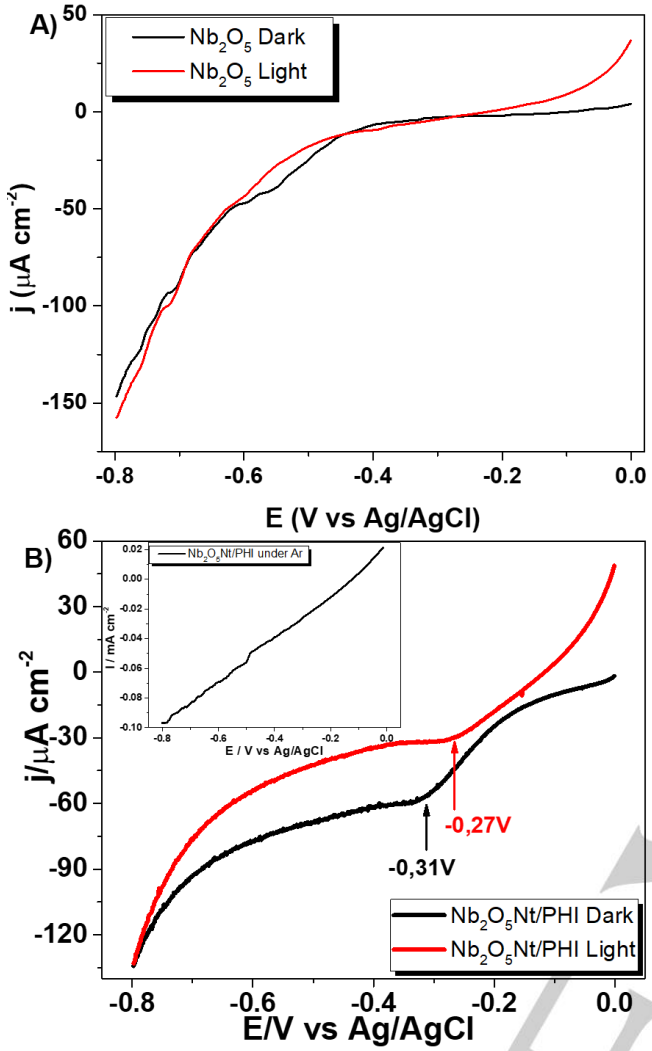

Figure 6. LSV under dark (black lines) and light (red lines) conditions for **A)** Nb_2O_5Nt and **B)** Nb_2O_5Nt/PHI performed using 0.1 mol L^{-1} PBS buffer (pH 7.0) solution saturated with N_2 gas as supporting electrolyte and inset saturated with Ar gas.

Taking into consideration the facts that (i) the cathodic current is observed for the unmodified material just after -0.2 V vs Ag/AgCl, (ii) there is evidence that the adsorption of N_2 happens around -0.3 $V_{(Ag/AgCl,3M)}$, and (iii) the OCP of both photoelectrodes; the reduction of N_2 was investigated under the potential -0.3 V and -0.4 $V_{(Ag/AgCl,3M)}$. Potentials higher than that were not investigated based on the results observed in this work and the literature.[10,12,43] The N_2RR using photoelectrocatalysis technique takes place under low negative potentials, as can be observed in diverse studies that are discussed in Table 1 further ahead.

The reduction of N_2 was performed using the Nb_2O_5Nt/PHI and compared with the catalyst without modification. The reaction was conducted in an H-cell with 0.1 mol L^{-1} PBS buffer solution saturated with N_2 on the cathodic side and 0.05 mol L^{-1} H_2SO_4 in the anodic compartment. The NH_3 production was investigated along the time of reduction reaction using a colorimetric method and the results obtained applying different conditions are presented in Figure 7. The green bars present the absorbance from the colorimetric detection test after 4 hours of N2RR, while the orange bars correspond to the amount of generated NH_3. The N2RR was investigated by applying the Nb_2O_5Nt/PHI photocatalyst under -0.3 V and -0.4 $V_{(Ag/AgCl,3M)}$, with an expressive higher formation of NH_3 under the lower negative potential. The obtained amount of NH_3 applying -0.4 $V_{(Ag/AgCl,3M)}$ (0.023 mmol L^{-1} cm^{-2} h^{-1}) is about six times lower than the amount obtained using -0.3 $V_{(Ag/AgCl,3M)}$ (0.156 mmol L^{-1} cm^{-2} h^{-1}). The NH_3 production was compared to bare niobium pentoxide at -0.3 $V_{(Ag/AgCl,3M)}$, and as expected, the PHI is essential to the success of the N2RR, without this modification the NH_3 synthesis decreased around eight times under the same conditions. Aiming to further investigate the material, the Nb_2O_5Nt/PHI was applied to the electrocatalytic reduction (EC, without light incidence), photocatalytic reduction (PC, without bias potential), and both techniques showed low NH_3 values, being 0.005 and 0.007 mmol L^{-1} cm^{-2} h^{-1} for EC and PC, respectively, evidencing the superior performance of the photoelectrocatalysis technique. Furthermore, the same photoelectrocatalytic conditions were employed (1 sun, PBS buffer, -0.3 $V_{(Ag/AgCl,3M)}$), but under a supporting electrolyte saturated with Ar instead N_2. As the absorbance after 4 h of measurement was below the detection limit of the colorimetric test, it was possible to conclude that the NH_3 production occurs exclusively from the N2RR and not by any possible decomposition of PHI structure. Carbon nitrides have been reported with no structure decomposition in a wide range of potentials,[44,45] and the present study proves that the use of a light input concomitant to the electrochemistry is not an issue for carbon nitrides.

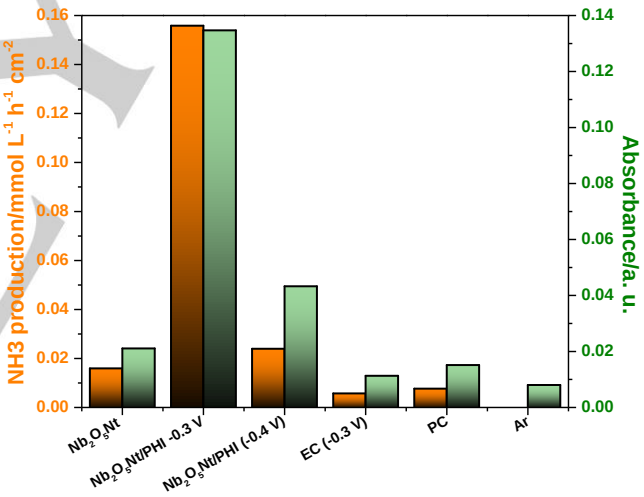

Figure 7. Ammonia production (orange bars) and absorbance obtained in the colorimetric quantification of generated ammonia (green bars) for Nb_2O_5Nt and Nb_2O_5Nt/PHI catalyst under different conditions: PEC using -0.3 V and 1 sun as well -0.4 V and 1 sun, and the blank conditions: EC at -0.3V, PC and PEC under Ar instead N2 (yellow).

For the reduction conducted under -0.3 V vs Ag/AgCl, which was the best potential for the reaction, the amount of NH_3 obtained in Nb_2O_5Nt/PHI was 0.156 mmol L^{-1} h^{-1} cm^{-2}, which lead to a Solar-to-Chemical-Conversion (SCC) of 14.66%, while Nb_2O_5Nt without modification generated 0.0159 mmol L^{-1} h^{-1} cm^{-2} of NH_3 with an SCC of 1.49%. This efficiency parameter stands out when compared to the SCC for the ammonia photocatalytic generation,[46] or even with other value-added products obtention, such as hydrogen[47,48] and H_2O_2.[49] The modification of the Nb_2O_5Nt surface with PHI was essential to perform the reduction of N_2, generating a concentration of NH_3 10-fold higher after the junction.

The modification of the Nb_2O_5Nt with PHI was not just essential to the N2RR process, but also to improve the stability of the nanotubular electrode, as can be observed in Figure 8a which presents the stability of both photocatalysts after 240 min of chronoamperometry under a potential of -0.3 $V_{(Ag/AgCl,3M)}$ and 1 sun illumination. The Nb_2O_5Nt semiconductor presented low stability, with a progressive decrease of the photocurrent density at the end of the analysis when compared to the initial seconds. This increase in the photocurrent to more negative values indicates a surface modification of the photocatalyst material along the time of the reaction, possibly a conversion of Nb_2O_5 for p-type NbO

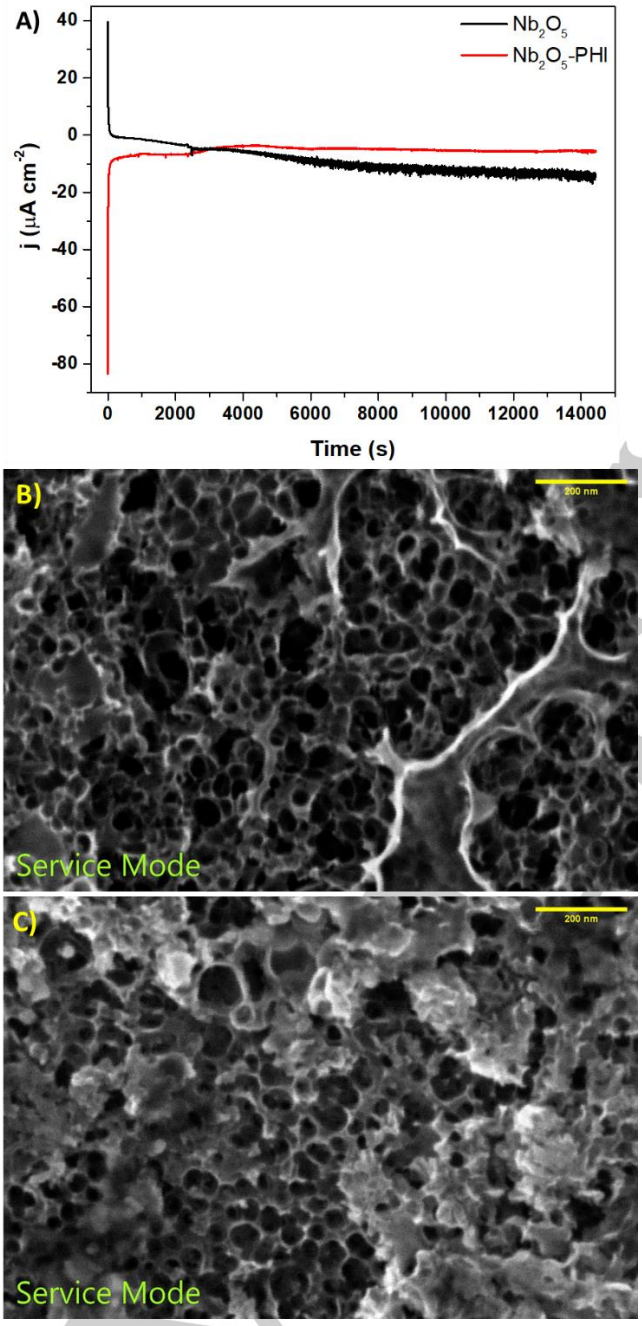

Figure 8. A) Stability test for 240 min under 1 sunlight incidence and potential of -0.3 $V_{(Ag/AgCl,3M)}$ for both Nb_2O_5Nt (black line) and Nb_2O_5Nt/PHI (red line) photocatalyst and SEM top view images for **B)** Nb_2O_5Nt and **C)** Nb_2O_5Nt/PHI after the stability test.

semiconductor.[50,51] On the other hand, the heterojunction of the Nb_2O_5Nt with PHI contributes to better stability of the photocatalyst, leading to only a 16% change in the photocurrent density along the 240 min of analysis.

The top view images of the Nb_2O_5Nt and Nb_2O_5Nt/PHI after the stability test are presented in Figures 8b and 8c. The Nb_2O_5Nt deterioration after 4 h of light and the potential incidence is easily observed (Figure 8b). Initially, the nanotubes are highly ordered (Figure 1a) and after the stability test, there is the presence of broken tubes and valley regions. On the other hand, with the insertion of PHI in the Nb_2O_5Nt surface, the nanotubes are preserved (Figure 8c) though the distribution of PHI has been changed compared with the catalyst before use (Figure 1b). The stability of the Nb_2O_5Nt/PHI after the stability reaction is reinforced by the XRD presented in Figure S2 where is possible to observe that the orthorhombic structure of Nb_2O_5Nt was not modified, despite a new peak which comes to be observed at 70° corresponding to the (112) plane. The PHI peak is still present in the diffractogram, however with a small intensity.

There are few works in the literature reporting carbon nitrides for N2RR, most of them are restricted to electrocatalysis and photocatalytic process, and the combination of both techniques is still rarely used for N2RR, rarer applying carbon nitrides-based photocatalysts. Table 1 compares the results presented in this work with previous data on NH_3 production involving carbon nitride materials. It is possible to conclude that the present results can be considered a benchmark amongst carbon nitride-based catalysts.

Is noteworthy to consider the synergic effect between PHI and Nb_2O_5 nanotubes, in addition to preserving the oxide structure, PHI also favors the N_2 adsorption for further reduction. Based on the performance observed for the N2RR, and on the band positioning of both materials, Figure 9 proposes a pathway of the materials acting as a Z-scheme to favor the photoelectrocatalytic ammonia generation. As occurs an accumulation of the photogenerated electrons in the PHI CB, the photocathode drives the ammonia production while the photogenerated holes are conducted to the anodic compartment through the external circuit to perform oxidation reactions.

Table 1. Comparison of N_2 reduction data from the literature with other carbon nitride-based catalysts at room temperature with NH_3.

Catalyst	Experimental conditions	Ammonia yield	Ref.
N_{vac}-PCN	Electrocatalytic, 0.1 M HCl electrolyte, -0.3 V_{RHE}	0.17 μmol $mg_{cat.}^{-1}$ h^{-1}	[43]
Mo_1-PCN	Photocatalytic, 300 W Xe lamp, ethanol as a scavenger	830 μmol g_{cat}^{-1} h^{-1}	[52]
P-dopped PCN	Photocatalytic, visible light	0.1 % SCC[a]	[46]
O_{vac}-$In(OH)_3$/CN	Photocatalytic, 300 W Xe lamp, triethanolamine as a scavenger	3.81 mmol L^{-1} h^{-1} g_{cat}^{-1}	[53]
g-C_3N_4/$ZnFe_2O_4$	Photocatalytic, visible light	0.0611 mmol L^{-1} h^{-1}	[54]
$MoSe_2$@g-C_3N_4	Photoelectrocatalytic, visible light, 0.1 M KOH electrolyte, -0.3 V_{RHE}	7.72 μmol $h^{-1}cm^{-2}$	[12]

Nb_2O_5/PHI	Photoelectrocatalytic, solar simulator, PBS buffer, -0.3 $V_{(Ag/AgCl,3M)}$	0.156 mmol L^{-1} h^{-1} cm^{-2}	This work

[a] Efficiency parameter based on the energy input conversion to ammonia.

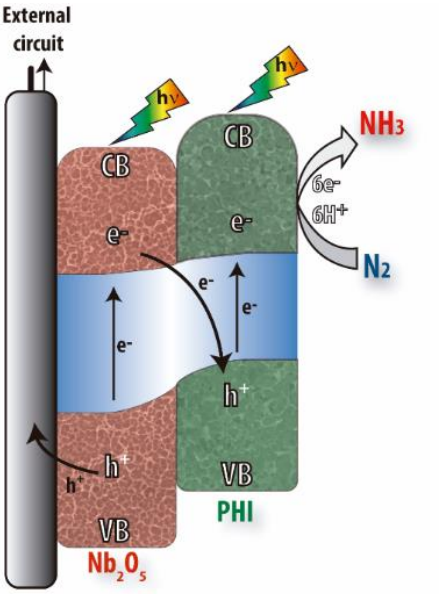

Figure 9. Proposed pathway for N_2 reduction over Nb_2O_5Nt/PHI photocathode.

Conclusion

The present work described the obtention and characterization of the new heterojunction Nb_2O_5Nt/PHI photocathode, where niobium pentoxide was prepared by anodization, and the PHI was deposited over the nanotubes by spin coating. After the PHI deposition, was possible to observe a thin film covering the surface of Nb_2O_5 nanotubes. This coating improved the electrode stability, as well as the SCC for ammonia yield by tenfold when compared to bare Nb_2O_5Nt. Besides the better stability, the improved performance is due to a cooperative effect from both materials, where the pyridinic nitrogens on PHI favor the N_2 adsorption and weakens the stable triple bond for posterior reduction. Also, due to the band position, the materials formed a direct Z-scheme, with the accumulation of the photogenerated electrons in the PHI structure, which explains the better performance in N2RR. Furthermore, the conditions employed are also worth mentioning, the reaction was performed under mild conditions, such as solar simulated light, neutral pH media, and low overpotential (-0.3 $V_{Ag/AgCl}$). Thus, the system configures an environmentally friendly and effective method to obtain a fundamental resource such as ammonia.

Experimental Section

Synthesis of the photoelectrodes. The Nb_2O_5 nanotubes synthesis procedure is extensively discussed in companion work.[14] Briefly, a 1.0 x 1.0 cm Nb foil (0.127 mm thick, 99.8% metal basis, Alfa Aesar) was cleaned in an ultrasonic bath to remove any oxide layer as follows: H_2SO_4 (50% v/v), acetone, isopropanol, and distilled water, in steps of 20 minutes of sonication for each compound. After an oven dry, the Nb foil was submitted to anodization (Keithley, 1100V SourceMeter®), applying 90 V of potential for 120 min in a one-compartment cell using two Pt grids as counter electrodes. For that, the supporting electrolyte consisted of 0.8 mol L^{-1} NH_4F in glycerol with 2% (v/v) H_2O. After anodization, the Nb foil was rinsed with deionized water, dried with N_2, and heated from room temperature to 450 °C at a rate of 2 °C min^{-1}, maintaining for 60 min, then allowing the system to cool down.

PHI was synthesized according to the literature.[25] For that, 1 g of melamine was ball milled with 10 g of NaCl. The reaction mixture was oven heated, in a porcelain crucible, under nitrogen flow (5 L min^{-1}), at a heating rate of 2.3 °C min^{-1} up to 600 °C. The temperature was held for 4 h and then cooled down. The product was removed and washed by filtration with deionized water (1 L), and acetone (250 mL). Thus, the product was dried overnight in an oven at 60°C, obtaining PHI as a powder.

For the deposition of PHI over the Nb_2O_5 nanotubes, it was prepared an ethanolic solution with ethylcellulose to obtain a paste. For that, 0.15 g of PHI was suspended in 1 g of ethanol and 0.1 g of ethylcellulose. After complete homogenization, 0.1 mL of this paste was spin-coated over Nb_2O_5 for 30 s at 3000 rpm. This procedure was followed by thermal treatment heating from room temperature to 400 °C, at a rate of 5 °C min^{-1}, maintained at 400 °C for 20 min, then cooling the system, obtaining Nb_2O_5/PHI.

Characterization. The structure and morphology of the Nb_2O_5 nanotube decorated with PHI semiconductors were characterized using Scanning Electron Microscopy with Field-Emission Gun (FEG-SEM, Supra 35-VP, Carl Zeiss, Germany), Dual Beam Electron Microscopy with Focused ion beam (FIB-SEM, Fei, Helios Nanolab 600I), X-Ray Diffraction (XRD, Siemens AXS Analytics D5005 X-ray diffractometer), and elemental mapping analysis was performed in a tabletop microscope (Hitachi TM4000II), equipped with an EDS detector (Oxford - Xplore compact). Raman spectroscopy was performed on a Micro Raman spectrophotometer (Horiba iHR-550) with a 633 nm laser. Electrochemical impedance spectroscopy (EIS) was conducted at the open circuit potential (OCP), scanning a frequency range of 10 kHz to 10 mHz with an amplitude of 10 mV in $5.0x10^{-3}$ mol L^{-1} $Fe(CN)_6^{3-/4-}$ redox probe (0.1 mol L^{-1} KCl). Mott-Schottky analysis was performed by measuring impedance spectra of the samples in a potential range from -0.4 to -0.1 V vs Ag/AgCl, 10 mV potential amplitude, and frequencies of 5 kHz to 1 kHz. Photocurrent measurements were performed with linear sweep voltammograms (LSV), measured at 10 mV s^{-1}, using a commercial solar simulator lamp (Asahi - HAL-320), with an intensity of 100 mW cm^{-2} (1 sun) and a potentiostat/galvanostat (Autolab model PGSTAT 302, Metrohm). The band gap of the Nb_2O_5 nanotubes with and without modification was determined using NIR-UV-vis spectroscopy (Cary, 5E® spectrometer).

Photoelectrocatalytic reduction of N_2. The N_2 reduction reaction procedure was adapted from Brito and coworkers.[10] The photoelectrocatalytic reduction of N_2 was performed in a completely sealed H-cell with, a cooling system, a quartz window, and three electrodes. Figure 10 presents a representative scheme of the photochemical cell reactor. An $Ag/AgCl_{(3M)}$ electrode was used as the reference electrode (RE), a Pt wire as the counter electrode (CE), and the Nb_2O_5Nt with and without PHI as the working electrode (WE). The anodic compartment contained CE where the oxidation process generates the protons, and the cathodic compartment contained RE and WE where the reduction reaction produces N_2 radicals that react with the protons. Both compartments were separated by a proton exchange

nafion™ membrane (PEM). The supporting electrolyte in the anodic compartment was 0.05 mol L^{-1} H_2SO_4, while the reaction in the cathodic compartment was carried out in 40 mL of 0.1 mol L^{-1} PBS buffer (pH 7.0) solution saturated with N_2 gas that was bubbled throughout the entire experiment. A 30 mL acid trap of 0.005 mol L^{-1} H_3PO_4[55] was connected to the cathodic compartment for ammonia to be collected during the reaction. Photoelectrocatalysis was performed under different potentials and 1 sunlight irradiation (Xe lamp and AM 1.5 G filter, Asahi - Hal-320, 100 mW cm^{-2}). Aliquots were collected from the acid trap during the reaction time and the amount of NH_3 in all of them was analyzed by a colorimetric method of indophenol blue using the Merck Spectroquant® commercial kit.

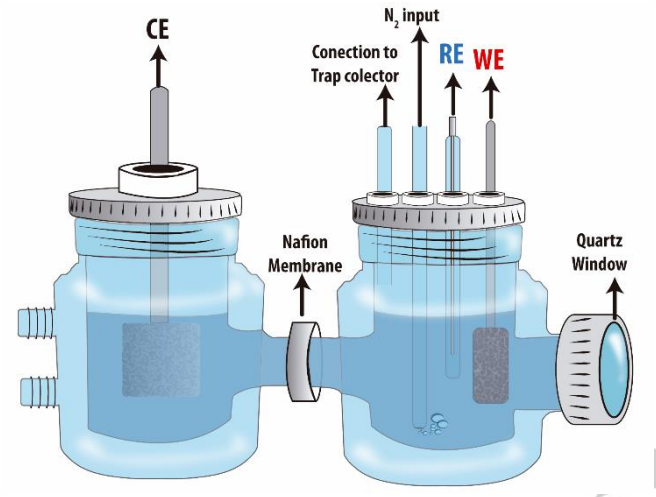

Figure 10. Representative scheme of the photochemical reactor for the N_2 reduction reaction.

To determine the Solar-to-Chemical-Conversion (SCC) efficiency it was employed the following equation:

$$SCC = \frac{[\Delta G\ NH_3(J\ mol^{-1})]x[NH_3(mol)]}{[Energy\ input(W)]x[Reaction\ time(s)]}x100$$

The free energy for NH_3 formation is 339 kJ mol^{-1}.[46] The irradiance from the solar simulator is 1000 W m^{-2}, and the electrode area is 1.96×10^{-7} m^2, which leads to a power input of 0.196 mW.

Acknowledgments

Funding: This work was supported by São Paulo Research Foundation, FAPESP [grant numbers #2018/02950-0, #2018/16401-8, #2013/07296-2, and #2017/11986-5], Coordenação de Aperfeiçoamento de Pessoal de Nível Superior - Brasil, CAPES [grant number 001], Conselho Nacional de Pesquisa e Desenvolvimento, CNPq [grant number #406156/2022-0], and INCT-DATREM [grant number #465571/2014-0]. The authors thank the Laboratory of Structural Characterization, LCE/DEMa/UFSCar, for the general facilities. Shell and the strategic importance of the support given by ANP (Brazil's National Oil, Natural Gas, and Biofuels Agency) through the R&D levy regulation.

Keywords: Polymeric carbon nitrides • Poly(Heptazine Imide) • Ammonia synthesis • Photoelectrocatalysis • N_2 reduction

[1] J. W. Erisman, M. A. Sutton, J. Galloway, Z. Klimont, W. Winiwarter, *Nat. Geosci.* **2008**, *1*, 636–639. 10.1038/ngeo325

[2] M. Li, X. Liu, L. Wang, F. Hou, S. X. Dou, J. Liang, *EcoMat* **2021**, *3*, 1–26. 10.1002/eom2.12096

[3] A. J. Medford, M. C. Hatzell, *ACS Catal.* **2017**, *7*, 2624–2643. 10.1021/acscatal.7b00439

[4] K. E. Dalle, J. Warnan, J. J. Leung, B. Reuillard, I. S. Karmel, E. Reisner, *Chem. Rev.* **2019**, *119*, 2752–2875. 10.1021/acs.chemrev.8b00392

[5] X. Liu, A. Elgowainy, M. Wang, *Green Chem.* **2020**, *22*, 5751–5761. 10.1039/D0GC02301A

[6] C. Xiao, H. Hu, X. Zhang, D. R. MacFarlane, *ACS Sustain. Chem. Eng.* **2017**, *5*, 10858–10863. 10.1021/acssuschemeng.7b01742

[7] T. Fei, L. Yu, Z. Liu, Y. Song, F. Xu, Z. Mo, C. Liu, J. Deng, H. Ji, M. Cheng, Y. Lei, H. Xu, H. Li, *J. Colloid Interface Sci.* **2019**, *557*, 498–505. 10.1016/j.jcis.2019.09.011

[8] W. Fang, J. Zhao, T. Wu, Y. Huang, L. Yang, C. Liu, Q. Zhang, K. Huang, Q. Yan, *J. Mater. Chem. A,* **2020**, *8*, 5913–5918. 10.1039/D0TA00676A

[9] S. Chen, S. Perathoner, C. Ampelli, C. Mebrahtu, D. Su, G. Centi, *ACS Sustain. Chem. Eng.* **2017**, *5*, 7393–7400. 10.1021/acssuschemeng.7b01742

[10] J. F. de Brito, M. B. Costa, K. Rajeshwar, L. H. Mascaro, *Electrochim. Acta* **2022**, *421*, 140475. 10.1016/j.electacta.2022.140475

[11] W. Ye, M. Arif, X. Fang, M. A. Mushtaq, X. Chen, D. Yan, *ACS Appl. Mater. Interfaces* **2019**, *11*, 28809–28817. 10.1021/acsami.9b06596

[12] M. A. Mushtaq, M. Arif, X. Fang, G. Yasin, W. Ye, M. Basharat, B. Zhou, S. Yang, S. Ji, D. Yan, *J. Mater. Chem. A,* **2021**, *9*, 2742–2753. 10.1039/d0ta10620h

[13] Z. Q. Chu, C. Stampfl, X. M. Duan, *J. Phys. Chem. C* **2019**, *123*, 28739–28743. 10.1021/acs.jpcc.9b08169

[14] J. F. de Brito, L. H. Mascaro, *J. Mater. Sci.* **2020**. 10.1007/s10853-020-05317-8.

[15] V. Galstyan, E. Comini, G. Faglia, G. Sberveglieri, *CrystEngComm* **2014**, *16*, 10273–10279. 10.1039/c4ce01540a

[16] M. Yang, X. Zhao, S. Zheng, X. Liu, B. Jin, H. Li, Y. Gan, *J. Electroanal. Chem.* **2017**, *791*, 17–22. 10.1016/j.jelechem.2017.03.009.

[17] C. Adán, J. Marugán, E. Sánchez, C. Pablos, R. Van Grieken, *Electrochim. Acta* **2016**, *191*, 521–529. 10.1016/j.electacta.2016.01.088

[18] R. P. Lynch, A. Ghicov, P. Schmuki, *J. Electrochem. Soc.* **2010**, *157*, G76. 10.1149/1.3276455

[19] J. Liu, D. Xue, K. Li, *Nanoscale Res. Lett.* **2011**, *6*, 1–8. 10.1186/1556-276X-6-138

[20] W. Wei, K. Lee, S. Shaw, P. Schmuki, *Chem. Commun.* **2012**, *48*, 4244. 10.1186/1556-276X-6-138

[21] Y. Liu, Y. Su, X. Quan, X. Fan, S. Chen, H. Yu, H. Zhao, Y. Zhang, J. Zhao, *ACS Catal.* **2018**, *8*, 1186–1191. 10.1016/j.jallcom.2021.158731

[22] D. W. Stephan, *Acc. Chem. Res.* **2015**, *48*, 306–316. 10.1016/j.jallcom.2021.158731

[23] I. F. Teixeira, E. C. M. Barbosa, S. C. E. Tsang, P. H. C. Camargo, *Chem. Soc. Rev.* **2018**, *47*, 7783–7817. 10.1016/j.jallcom.2021.158731

[24] D. Zhang, W. He, J. Ye, X. Gao, D. Wang, J. Song, *Small* **2021**, *17*, 2005149. 10.1002/smll.202005149

[25] Z. Chen, A. Savateev, S. Pronkin, V. Papaefthimiou, C. Wolff, M. G. Willinger, E. Willinger, D. Neher, M. Antonietti, D. Dontsova, *Adv. Mater.* **2017**, *29*, 1700555. 10.1002/adma.201700555

[26] H. Schlomberg, J. Kröger, G. Savasci, M. W. Terban, S. Bette, I. Moudrakovski, V. Duppel, F. Podjaski, R. Siegel, J. Senker, R. E. Dinnebier, C. Ochsenfeld, B. V. Lotsch, *Chem. Mater.* **2019**, *31*, 7478–7486. 10.1021/acs.chemmater.9b02199

[27] S. F. Blaskievicz, H. L. S. Santos, I. F. Teixeira, J. L. Bott-Neto, P. S. Fernández, L. H. Mascaro, *Mater. Today Nano* **2022**, *18*, 100192. 10.1021/acs.chemmater.9b02199

[28] H. Kreissl, M. Li, Y.-K. Peng, K. Nakagawa, T. Hooper, J. Hanna, A. Shepherd, W. Tai-Sing, Y.-L. Soo, S. C. Tsang, *J. Am. Chem. Soc.* **2017**, *139*, 10.1021/jacs.7b06856.

[29] M. P. F. Graça, A. Meireles, C. Nico, M. A. Valente, *J. Alloys Compd.* **2013**, *553*, 177–182. 10.1021/acs.chemmater.9b02199

[30] C. Nico, M. R. N. Soares, J. Rodrigues, M. Matos, R. Monteiro, M. P. F. Graça, M. A. Valente, F. M. Costa, T. Monteiro, *J. Phys. Chem. C* **2011**, *115*, 4879–4886. 10.1021/acs.chemmater.9b02199

[31] X. Bai, L. Wang, Y. Wang, W. Yao, Y. Zhu, *Appl. Catal. B Environ.* **2014**, *152*, 262–270. 10.1021/acs.chemmater.9b02199

[32] A. B. Jorge, D. J. Martin, M. T. S. Dhanoa, A. S. Rahman, N. Makwana, J. Tang, A. Sella, F. Corà, S. Firth, J. A. Darr, *J. Phys. Chem. C* **2013**, *117*, 7178–7185. 10.1021/acs.chemmater.9b02199

[33] K. K. Upadhyay, T. Nguyen, T. M. Silva, M. J. Carmezim, M. F. Montemor, *Mater. Chem. Phys.* **2018**, *216*, 413–420. 10.1021/acs.chemmater.9b02199

[34] M. Medina, P. G. Corradini, J. F. de Brito, H. L. Sousa Santos, L. H. Mascaro, *J. Electrochem. Soc.* **2022**, *169*, 026519. 10.1021/acs.chemmater.9b02199

[35] S. U. Khan, J. A. L. Perini, S. Hussain, H. Khan, S. Khan, M. V. Boldrin Zanoni, *Chemosphere* **2020**, *257*, 10.1016/j.chemosphere.2020.127164.

[36] S. N. S. Nasir, N. A. Mohamed, M. A. Tukimon, M. F. M. Noh, N. A. Arzaee, M. A. M. Teridi, *Phys. B Condens. Matter* **2021**, *604*, 412719. 10.1021/acs.chemmater.9b02199

[37] F. Idrees, R. Dillert, D. Bahnemann, F. Butt, M. Tahir, *Catalysts* **2019**, *9*, 169. 10.1021/acs.chemmater.9b02199

[38] R. Abdul Rani, A. S. Zoolfakar, J. Subbiah, J. Z. Ou, K. Kalantar-Zadeh, *Electrochem. commun.* **2014**, *40*, 20–23. 10.1021/acs.chemmater.9b02199

[39] T.-A. Bu, Y.-C. Hao, W.-Y. Gao, X. Su, L.-W. Chen, N. Zhang, A.-X. Yin, *Nanoscale* **2019**, *11*, 10072–10079. 10.1021/acs.chemmater.9b02199

[40] J. F. de Brito, M. V. B. Zanoni, *Chem. Eng. J.* **2017**, *318*, 264–271. 10.1016/j.cej.2016.08.033

[41] S. Kumar, N. Yadav, P. Kumar, A. K. Ganguli, *Inorg. Chem.* **2018**, *57*, 15112–15122. 10.1021/acs.inorgchem.8b02264

[42] W. Xu, W. Tian, L. Meng, F. Cao, L. Li, *Adv. Energy Mater.* **2021**, *11*, 2003500. 10.1002/aenm.202003500

[43] G. Peng, J. Wu, M. Wang, J. Niklas, H. Zhou, C. Liu, *Nano Lett.* **2020**, *20*, 2879–2885. 10.1021/acs.nanolett.0c00698.

[44] C. Lv, Y. Qian, C. Yan, Y. Ding, Y. Liu, G. Chen, G. Yu, *Angew. Chemie Int. Ed.* **2018**, *57*, 10246–10250. 10.1002/anie.201806386

[45] G. Peng, J. Wu, M. Wang, J. Niklas, H. Zhou, C. Liu, *Nano Lett.* **2020**, *20*, 2879–2885. 10.1021/acs.nanolett.0c00698

[46] Y. Shiraishi, S. Shiota, Y. Kofuji, M. Hashimoto, K. Chishiro, H. Hirakawa, S. Tanaka, S. Ichikawa, T. Hirai, *ACS Appl. Energy Mater.* **2018**, *1*, 4169–4177.

[47] J. Kubota, K. Domen, *Interface Mag.* **2013**, *22*, 57–62.

[48] K. Maeda, K. Teramura, D. Lu, T. Takata, N. Saito, Y. Inoue, K. Domen, *Nature* **2006**, *440*, 295–295. 10.1021/acsaem.8b00829

[49] Y. Kofuji, Y. Isobe, Y. Shiraishi, H. Sakamoto, S. Tanaka, S. Ichikawa, T. Hirai, *J. Am. Chem. Soc.* **2016**, *138*, 10019–10025. 10.1021/jacs.6b05806

[50] Y. Erarslanoglu, I. Onal, T. Dogu, S. Senkan, *Catal. Letters* **1996**, *38*, 215–218. 10.1007/BF00806571

[51] M. Delheusy, A. Stierle, N. Kasper, R. P. Kurta, A. Vlad, H. Dosch, C. Antoine, A. Resta, E. Lundgren, J. Andersen, *Appl. Phys. Lett.* **2008**, *92*, 101911. 10.1063/1.2889474

[52] X.-W. Guo, S.-M. Chen, H.-J. Wang, Z.-M. Zhang, H. Lin, L. Song, T.-B. Lu, *J. Mater. Chem. A* **2019**, *7*, 19831–19837. 10.1039/C9TA06653E

[53] J. Fan, M. Zuo, Z. Ding, Z. Zhao, J. Liu, B. Sun, *Chem. Eng. J.* **2020**, *396*, 125263. 10.1039/C9TA06653E

[54] X. Rong, S. Liu, M. Xie, Z. Liu, Z. Wu, X. Zhou, X. Qiu, J. Wei, *Mater. Res. Bull.* **2020**, *127*, 110853. 10.1016/j.materresbull.2020.110853

[55] A. L. Woodley, C. F. Drury, W. D. Reynolds, W. Calder, X. M. Yang, T. O. Oloya, *Can. J. Soil Sci.* **2018**, *98*, 193–199. 10.1139/cjss-2017-0081

10.1002/cctc.202201610

Table of contents

Looking to other possibilities to produce NH_3 than the Haber-Bosch process, this work describes the reduction of N_2 by photoelectrocatalysis using poly(heptazine imide) (PHI) deposited on niobium pentoxide oxide (Nb_2O_5) photocatalyst. The photoelectrosynthesis of NH_3 was carried out using mild and green conditions improving 10-fold the production by the presence of PHI compared to bare Nb_2O_5.

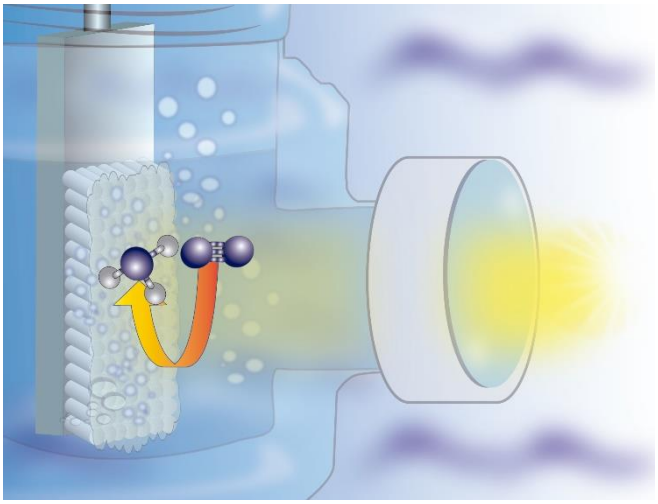

10.1002/cctc.202201610